

# Active Microrheology and Dynamic Phases for Pattern Forming Systems with Competing Interactions

C. Reichhardt and C. J. O. Reichhardt

*Theoretical Division and Center for Nonlinear Studies,  
Los Alamos National Laboratory, Los Alamos, New Mexico 87545, USA*

(Dated: January 10, 2025)

We consider the driven dynamics of a probe particle moving through an assembly of particles with competing long-range repulsive and short-range attractive interactions, which form crystal, stripe, labyrinth, and bubble states as the ratio of attraction to repulsion is varied. We show that the probe particle exhibits a depinning-like threshold from an elastic regime, where the probe particle is trapped by interactions with the other particles, to a plastic flow regime, where the probe particle can break bonds in the surrounding medium. For a fixed particle density, the depinning threshold and sliding velocity of the probe particle vary nonmonotonically as the attraction term is increased. A velocity minimum appears near the crystal to stripe crossover, and there is a significant increase in the depinning threshold in the bubble regime when the probe particle is strongly confined inside the bubbles. For fixed attractive interaction but increasing particle density, the behavior is also nonmonotonic and there are jumps and drops in the velocity and depinning threshold corresponding to points at which the system transitions between different structures. There are also several distinct flow states that can be characterized by the amount of plastic deformation induced by the probe particle in the surrounding medium. Each flow state generates a different amount of effective drag on the probe particle, and there can be jumps in the velocity-force curve at transitions between the states. We also find that when oriented stripes are present, the probe particle can move along the stripe in an edge transport state that has a finite Hall angle.

## I. INTRODUCTION

In active rheology, a probe particle is driven through an assembly of other particles and produces a response that depends on the drive amplitude and the nature of the surrounding medium, which may be solid or fluid-like [1–15]. For colloidal assemblies that are in a glass or crystalline state, there can be a threshold driving force that must be applied to the probe particle so that it can transition from trapped to flowing [1, 2, 5, 16–18]. In granular matter, the drag on the probe particle can show a divergence as the critical jamming density is approached [19–21]. If there is some additional chirality in the system, the probe particles can exhibit odd viscosity behaviors such as a Hall effect that can depend on the magnitude of the driving force [22, 23]. In active matter systems, the drag on the probe particle depends on whether motility induced phase separation is occurring [24] and on how deformable the surroundings are [18].

Driving single particles through an assembly of other particles or over a disordered substrate has also been employed in hard condensed matter systems. For example, when dragging individual superconducting vortices [25–27] or skyrmions [28, 29], the probe particle interacts not only directly with the other particles but also with defects or pinning sites in the sample. In most active rheology systems, such as charged colloidal particles, superconducting vortices, and magnetic skyrmions, the particle-particle interaction potential is purely repulsive, and often consists of a very short range steric repulsion, as in uncharged colloidal particles and granular matter. A wide class of particle-based systems with competing long-range repulsive and short-range attractive interac-

tions exhibit a variety of pattern forming states as the relative attraction strength or particle density is varied, including anisotropic crystals, stripes, labyrinths, bubbles, and void lattices [30–42]. Similar patterns can form for systems in which the interactions are strictly repulsive when multiple length scales are present in the interaction potential [43–45]. This type of pattern formation occurs in a variety of soft matter systems such as colloidal assemblies, emulsions, binary fluids, and magnetic colloids with additional capillary interactions [44–46]. Stripe, bubble, and labyrinth patterns also occur in hard condensed matter systems such as electron liquid crystals [47–53], as well as several other charge-ordered states where competing interactions arise [54–56]. In multiple component superconductors, the vortex-vortex interactions can have multiple length scales, giving rise to mesoscale stripe and bubble-like ordering in the vortex structures [57–61]. Bubbles and stripes can also occur in magnetic systems such as skyrmion-supporting materials [62].

Despite the large number of systems in which bubble and stripe mesoscale ordering occurs, active microrheology of bubble and stripe states has not been studied before now. Here, we use large-scale numerical simulations of a probe particle driven through an assembly of particles that have a competing short-range attraction and long-range repulsion. Previous work with this type of interaction potential has shown that when the ratio of attraction to repulsion is varied or the density of the system is changed, the particles can transition among crystal, anisotropic crystal, stripe, void lattice, bubble, or labyrinthine phases [33, 36–38, 63, 64]. We demonstrate that active rheology of bubble and stripe systems

produces a wide variety of nonmonotonic motion thresholds, effective viscosities, and different flow states. The depinning threshold and type of flow of the probe particle depend on the patterns formed by the background particles and the magnitude of the driving force. There is a minimum in the depinning threshold near the crystal-to-stripe transition that occurs at fixed particle density for increasing attractive interactions. In the bubble state, there is a sharp increase in the depinning threshold because the probe particle can remain trapped inside a bubble for an extended range of drives, while at higher drives, there is a transition to a state in which the probe particle hops from bubble to bubble. We find that systems with competing interactions generally exhibit a greater variety of distinct flowing phases under active rheology than what is observed for purely repulsive interacting particles. In the stripe phase, the probe particle can create large plastic deformations in the stripe, leading to an increased drag effect; however, at high drives, the probe particle moves rapidly enough through the stripe that plastic deformations of the surrounding medium are reduced or no longer occur, producing a reduction in the number of fluctuations. These different dynamic phases are visible as changes in the velocity force curves and in the effective drag on the probe particle. The stripe state may adopt a disordered labyrinth configuration or an ordered stripe arrangement, depending on the interaction between the particles. In the ordered stripe state, there can be transport of the probe particle along the edge of the stripe, leading to the emergence of a finite Hall angle when the stripes are not aligned with the driving direction. At higher drives, the probe particle breaks through the stripe, leading to increased drag and a reduced Hall angle.

## II. SIMULATION

We consider a two-dimensional (2D) system of size  $L \times L$ , with  $L = 36$  and periodic boundary conditions in the  $x$ - and  $y$ -directions, containing  $N$  particles. The system density is  $\rho = N/L^2$ , and the particle-particle interaction potential has both a long-range repulsion and a short-range attraction. The probe particle is subjected to an external driving force  $F_D$  applied along the positive  $x$ -direction. The particle dynamics are obtained by integrating the following overdamped equation of motion:

$$\eta \frac{d\mathbf{R}_i}{dt} = - \sum_{j \neq i}^N \nabla V(R_{ij}) + \mathbf{F}_D^i \quad (1)$$

where  $R_{ij} = |\mathbf{R}_i - \mathbf{R}_j|$  is the distance between particles  $i$  and  $j$ . For the non-driven particles,  $\mathbf{F}_D^i = 0$ . The damping term is set to  $\eta = 1.0$ . The particle-particle interaction forces in the first term on the right hand side are obtained from the following potential:

$$V(R_{ij}) = \frac{1}{R_{ij}} - B \exp(-\kappa R_{ij}) . \quad (2)$$

The first term is the repulsive Coulomb interaction, and the second term is an attraction of strength  $B$  and inverse range  $\kappa$ . In this work we fix  $\kappa = 1.0$  while varying  $B$  and the density  $\rho$ ; however, we note that the type of patterns that form also depend on  $\kappa$ . The particle-particle interaction is repulsive at large distances and attractive at intermediate distances. At very short range, the Coulomb term is dominant, so the particles cannot all collapse onto a point. To treat the  $1/r$  interaction potential, we employ the real space Lekner summation technique, as used in previous work [32, 39]. The interaction potential in Eq. (2) has previously been shown to produce crystal, stripe, bubble, and void lattices as the attraction strength  $B$  is varied [32, 33, 38, 39, 65].

The initial particle configurations are obtained by placing the particles in a uniform triangular lattice and allowing them to relax into the patterned states. We have also performed simulated annealing by starting from a high temperature and slowly cooling the system to  $T = 0.0$ . We obtain similar patterns and dynamics for either initialization method. After the system has been initialized, we apply a driving force to the probe particle which we increase in increments of  $\delta F_D = 0.01$ . We spend 6200 to 10000 simulation time steps at each drive increment before increasing the drive again. We find the time-averaged velocity  $\langle V \rangle = \langle v_i \cdot \hat{\mathbf{x}} \rangle$  and  $\langle V_y \rangle = \langle v_i \cdot \hat{\mathbf{y}} \rangle$  of the probe particle both parallel and perpendicular to the driving direction.

## III. RESULTS

In Fig. 1, we show the locations and trajectories of the probe particle and the surrounding particles for a system in the disordered stripe regime at  $\rho = 0.44$  and  $B = 2.0$ . For  $F_D = 0.7$ , as shown in the figure, the probe particle can break through the stripe structure and cause distortions within it. Figure 2 illustrates representative examples of the different types of patterns that form as  $B$  and  $\rho$  are varied. There is a low density bubble phase for  $\rho = 0.0952$  and  $B = 1.8$  in Fig. 2(a), a crystal phase at  $\rho = 0.44$  and  $B = 1.6$  in Fig. 2(b), a bubble state for  $\rho = 0.44$  and  $B = 2.3$  in Fig. 2(c), and a void lattice at  $\rho = 0.52$  and  $B = 2.0$  in Fig. 2(d).

In Fig. 3, we plot some representative velocity-force curves for the probe particle from the system in Fig. 1 at a fixed density of  $\rho = 0.44$  for the crystal state at  $B = 0.2$ ,  $B = 0.8$ , and  $B = 1.9$ , the stripe state at  $B = 2.0$ , and the bubble state at  $B = 2.2$ ,  $B = 2.4$ ,  $B = 2.5$ , and  $B = 2.6$ . The black dashed line indicates the expected velocity-force curve for a freely moving particle. Each curve shows a finite threshold for motion followed by a sliding phase. The lowest depinning threshold occurs in the crystal regime at  $B = 1.9$ . The threshold increases rapidly upon entering the bubble state and continues to increase with increasing  $B$ . There are strong velocity fluctuations in the sliding phase when the particle is jumping from bubble to bubble. The velocity response

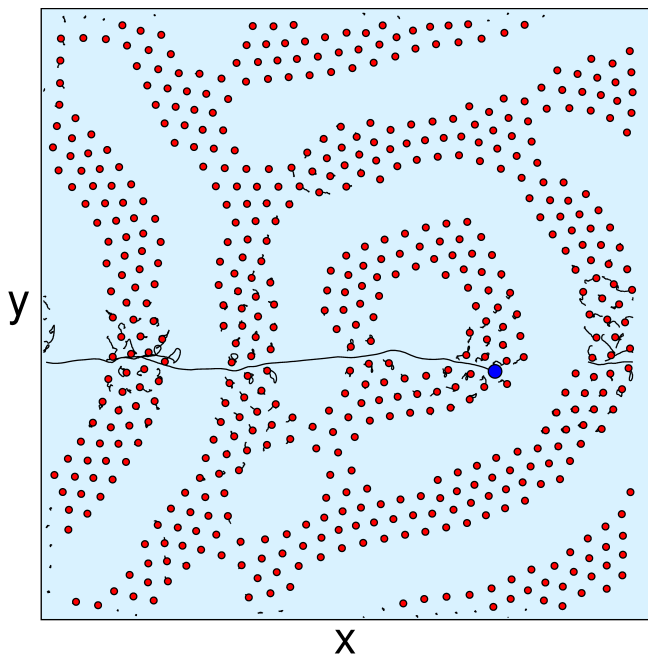


FIG. 1. Locations (dots) and trajectories (lines) of the probe particle (blue) and surrounding particles (red) in a system with  $\rho = 0.44$  and  $B = 2.0$  which forms a disordered stripe or labyrinthine phase. At  $F_D = 0.7$ , the probe particle can break through the stripe structure. In all results presented in this work, the probe particle and the background particles have the same size and the same charge, but the probe particle has been drawn larger than the background particles for clarity.

is nonmonotonic in the sliding regime, as exemplified by the fact that at  $F_D = 1.0$ , the velocity is low for  $B = 0.2$ , gradually increases with increasing  $B$  until  $B = 1.9$ , and then decreases again as  $B$  increases further.

In Fig. 4(a), we plot the threshold force  $F_c$  for motion versus  $B$  at fixed  $\rho = 0.44$ , and in Fig. 4(b) we show the corresponding value of  $\langle V \rangle$  at  $F_D = 1.0$ . The dashed lines indicate the boundaries of the crystal (Cr), stripe (Str), and bubble (B) states. We find that  $F_c$  decreases with increasing  $B$  in the crystal state, and that at the same time there is a linear increase in  $\langle V \rangle$ . A dip in  $F_c$  appears at  $B = 1.9$  just before the crystal-to-stripe transition, and is associated with a peak in  $\langle V \rangle$ . In the stripe phase,  $F_c$  increases with increasing  $B$  while  $\langle V \rangle$  drops, and there is a more rapid increase of  $F_c$  with increasing  $B$  in the bubble phase.

In the crystal regime, the probe particle depins and flows along a one-dimensional path between rows of the background particles, as shown in Fig. 5(a) at  $B = 0.2$  and  $F_D = 1.0$ . At lower drives, this channel motion is unstable and the probe particle moves by exchanging places with the background particles, resulting in the appearance of plastic deformations in the surrounding lattice, as illustrated in Fig. 5(b) at  $F_D = 0.3$ , just above the threshold drive. Since the plastic deformations result in an increased drag on the probe particle, there is a two-

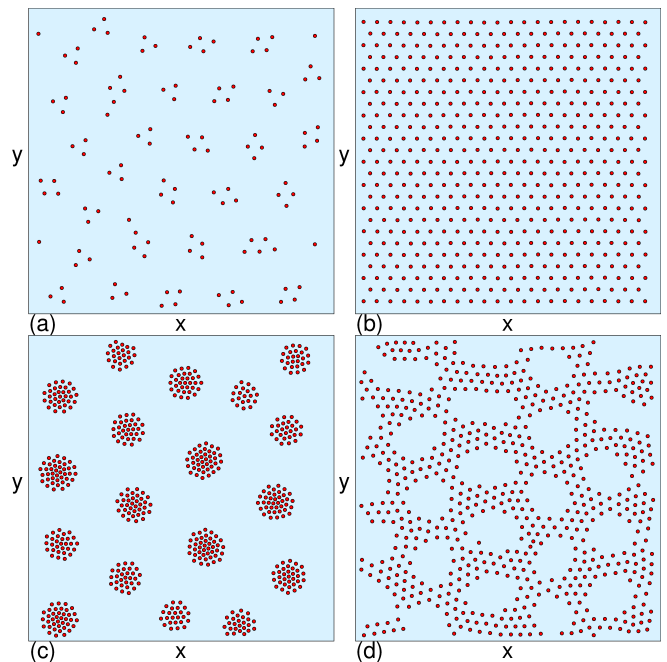


FIG. 2. Images of particle locations for representative examples of the different patterns that can form in the system for varied parameters. Here  $F_D = 0$ . (a) A low density bubble phase at  $\rho = 0.0952$  and  $B = 1.8$ . (b) A uniform crystal at  $B = 1.6$  and  $\rho = 0.44$ . (c) A bubble state at  $\rho = 0.44$  and  $B = 2.4$ . (d) A void lattice at  $\rho = 0.52$  and  $B = 2.0$ .

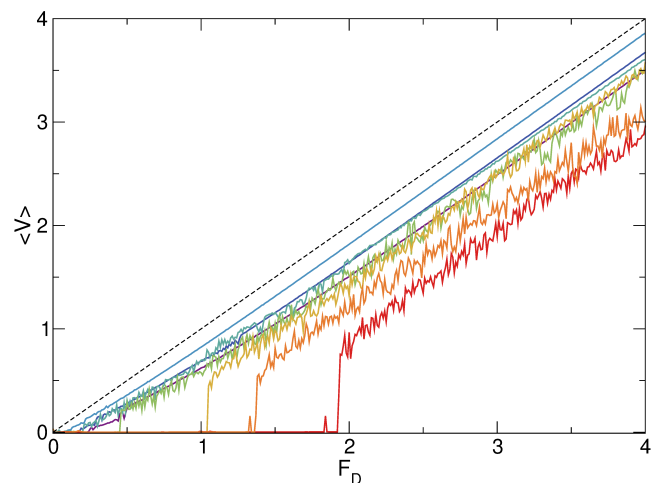


FIG. 3. The velocity-force curves  $\langle V \rangle$  vs  $F_D$  for the probe particle for the system from Fig. 1 with  $\rho = 0.44$  in the crystal state at  $B = 0.2$  (violet),  $B = 0.8$  (dark blue), and  $B = 1.9$  (light blue); the stripe state at  $B = 2.0$  (teal); and the bubble state at  $B = 2.2$  (green),  $B = 2.4$  (yellow),  $B = 2.5$  (orange), and  $B = 2.6$  (red). The lowest threshold and highest sliding velocity occur for  $B = 1.9$ . In the bubble phase, the depinning threshold increases with increasing  $B$ .

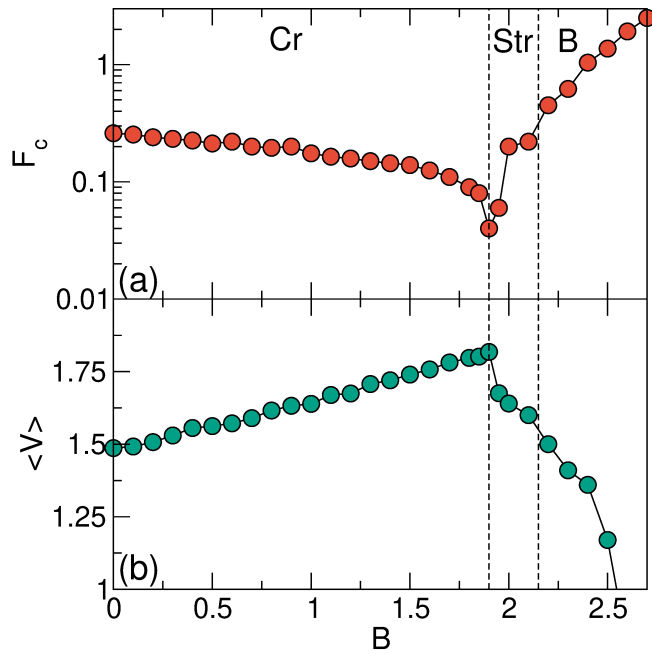


FIG. 4. (a) The depinning threshold  $F_c$  vs  $B$  for the system in Fig. 3 at  $\rho = 0.44$ . (b) The corresponding velocity  $\langle V \rangle$  at  $F_D = 1.0$  vs  $B$ . The dashed lines separate the crystal (Cr), stripe (Str), and bubble (B) phases. The threshold  $F_c$  passes through a minimum near the crystal to stripe transition and rapidly increases with increasing  $B$  in the bubble phase.

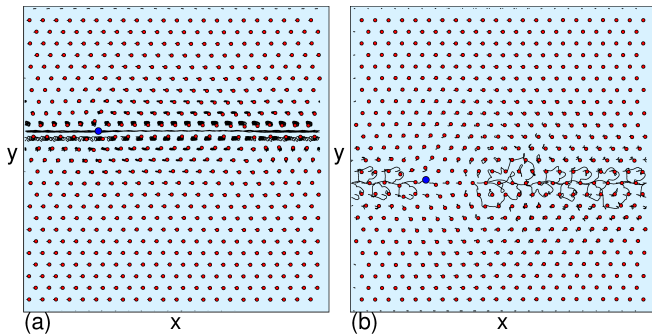


FIG. 5. Locations (dots) and trajectories (lines) of the probe particle (blue) and surrounding particles (red) in the crystal phase at  $\rho = 0.44$  and  $B = 0.2$ . (a) At  $F_D = 1.0$ , the probe particle passes between two rows of the background lattice without inducing plastic distortions. (b) At  $F_D = 0.3$ , just above the threshold  $F_c$ , the motion of the probe particle causes exchanges of the surrounding particles.

step feature in the velocity-force curve in Fig. 3, with a transition from a low drive motion with strong plastic distortions to an ordered flow at high drives.

For the stripe forming states, the probe particle is initially pinned since there are no rows providing easy-flow channels for motion. In order to translate, the probe particle must break out of the caging potential produced by the surrounding particles and force its way across the

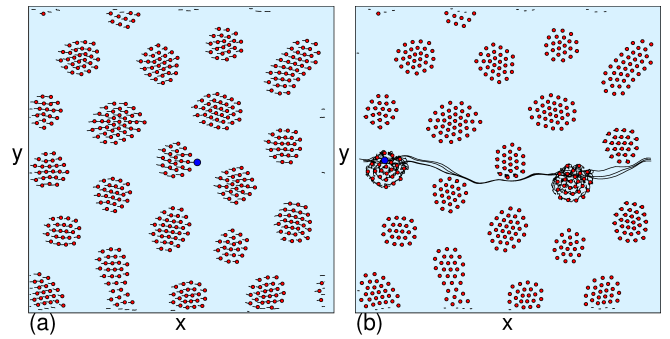


FIG. 6. Locations (dots) and trajectories (lines) of the probe particle (blue) and surrounding particles (red) in the bubble phase at  $\rho = 0.44$  and  $B = 2.4$ . (a) At  $F_D = 0.5$ , the probe particle remains trapped in a bubble, but the entire system translates as the bubble is dragged by the probe particle. (b) At  $F_D = 1.5$ , the probe particle jumps from bubble to bubble, creating plastic distortions in the bubbles.

stripe. This gives a larger value of  $F_c$  compared to the crystal regime and also increases the effective drag on the probe particle. In the bubble phase, the probe particle becomes trapped by the attractive portion of the interparticle interaction potential. As  $B$  increases, the attractive portion of the potential becomes stronger, increasing the barrier that must be overcome before the probe particle can jump from bubble to bubble. The dip in  $F_c$  near the crystal to stripe transition in Fig. 4(a) occurs when the attractive and repulsive forces on the probe particle are exactly balanced. Within the crystal phase, the probe particle is trapped by the caging effect from the repulsion of the other particles. For  $B = 0.0$ , this repulsive barrier is maximum. As  $B$  increases, the net repulsion is reduced since it is counterbalanced by the attractive force. The repulsion reaches its minimum at the onset of the stripe phase when the attractive part of the interaction force begins to dominate the caging of each particle, pulling the particles together into stripe structures. Like the background particles, the probe particle also becomes trapped by the attractive portion of the interaction potential. The magnitude of the attractive force increases when the stripes transform into bubbles, and as a result the threshold force  $F_c$  also increases at the stripe-to-bubble transition.

The trapped to flowing transition of the probe particle can also be viewed as an elastic to plastic transition. In Fig. 6 we show the trajectories of the particles for the system from Fig. 4 at  $\rho = 0.44$  and  $B = 2.4$  in the bubble phase. At  $F_D = 0.5$  in Fig. 6(a), the probe particle remains trapped in a bubble, but the entire system translates as this bubble is dragged. As indicated in the figure, the probe particle works its way to the front of the bubble that it is dragging. Here, the velocity of the probe particle is the same as the velocity of the background particles. The velocity in this elastic flow state decreases as  $1/N$ , where  $N$  is the number of particles in the system,

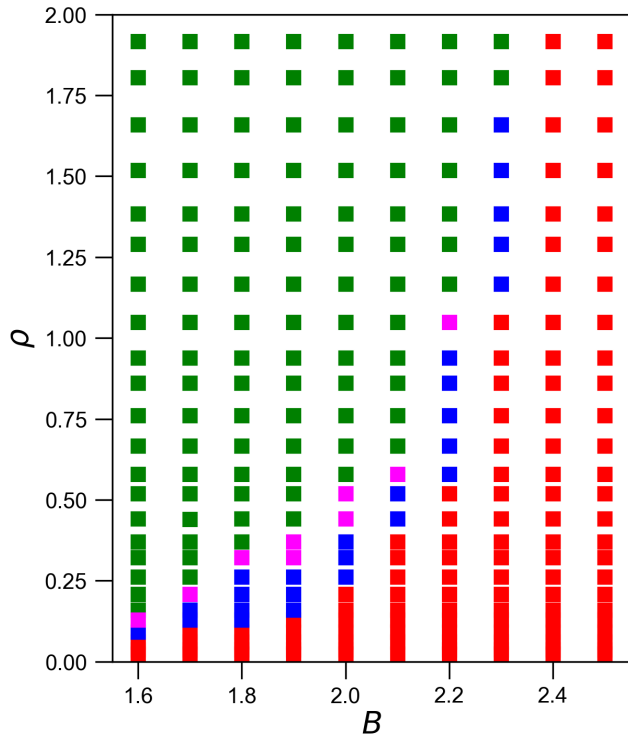


FIG. 7. Phase diagram as a function of  $\rho$  vs  $B$  in the absence of a driven probe particle highlighting where the system forms a triangular lattice (green), void lattice (magenta), stripes (blue), and bubbles (red).

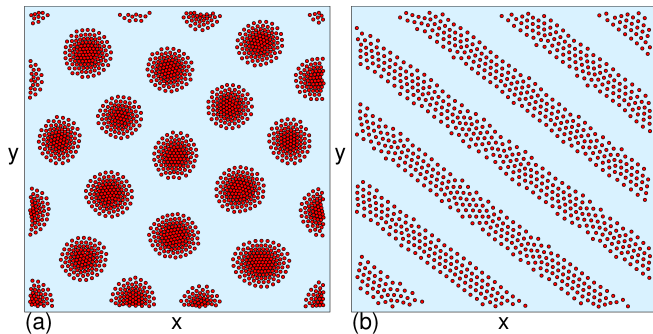


FIG. 8. Image of particle positions in the absence of a driven probe particle. (a) A bubble lattice at  $\rho = 1.8$  and  $B = 2.4$ , where there is a density gradient inside the individual bubbles. (b) An oriented stripe state at  $B = 2.2$  and  $\rho = 0.86$ .

so for large systems, the elastic velocity becomes very low and the system can be regarded as effectively pinned. In Fig. 6(b) at  $F_D = 1.5$ , the probe particle jumps from bubble to bubble, creating plastic distortions as it moves through the bubble lattice.

In Fig. 7, we plot a phase diagram as a function of  $\rho$  versus  $B$  highlighting where the system, in the absence of a probe particle, forms a triangular lattice, void lattice, stripes, and bubbles. Generally, for a fixed value

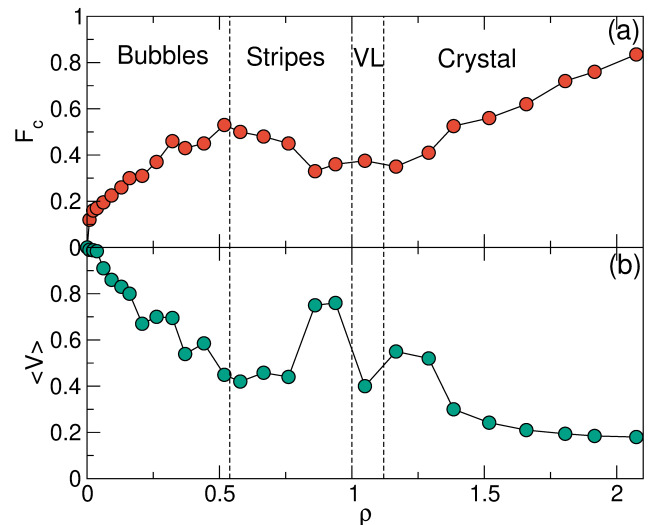


FIG. 9. (a) The depinning threshold  $F_c$  vs  $\rho$  for a system with  $B = 2.2$ . (b) The corresponding velocity  $\langle V \rangle$  at  $F_D = 1.0$  vs  $\rho$ . The dashed lines separate the bubbles, stripes, void lattice (VL), and crystal phases.

of  $B$ , clumps or bubbles appear when the density is low. The size and shape of the clump depend on the value of  $B$  and  $\rho$ . The clumps can be small or even disordered, as illustrated in Fig. 2(a), or large and form a lattice, as shown in Fig. 8(a) at  $\rho = 1.6$  and  $B = 2.4$ . There is also a density gradient within the large individual bubbles. The stripes can form disordered states, which is typical when the stripes are thin, but they can also form ordered structures at higher densities, as shown in Fig. 8(b) at  $B = 2.2$  and  $\rho = 0.86$ . In general, many of the stripe and bubble states exhibit aspects of metastability, so the ability to form ordered stripes versus disordered stripes in a real experiment would be controlled by the boundary conditions and the manner in which the system is prepared. The ordered stripe phase we illustrate in Fig. 8(b) could break into domains of different orientation if we considered a system of much larger size; however, we can still examine the active rheology for both ordered and disordered states since it should be possible to prepare fully ordered stripe systems in an experiment. The phase diagram in Fig. 7 indicates that as  $B$  increases, stripes and voids do not form until the density  $\rho$  is higher.

In Fig. 9(a), we plot the depinning threshold  $F_c$  versus  $\rho$  at a fixed  $B = 2.2$ , while in Fig. 9(b) we show the corresponding  $\langle V \rangle$  at a drive of  $F_D = 1.0$  versus  $\rho$ . The dashed lines show where transitions among the bubble, stripe, void lattice, and crystal states occur. At low  $\rho$  where the system forms small bubbles,  $F_c$  has a low value. As  $\rho$  increases, the bubbles grow in size, and the threshold  $F_c$  also increases until it reaches a local maximum at the bubble to stripe crossover near  $\rho = 0.525$ . The velocity drops to a local minimum in the disordered stripe phase that spans  $0.525 < \rho < 0.75$ . An oriented stripe phase appears for  $0.75 \leq \rho < 1.0$  that is associated

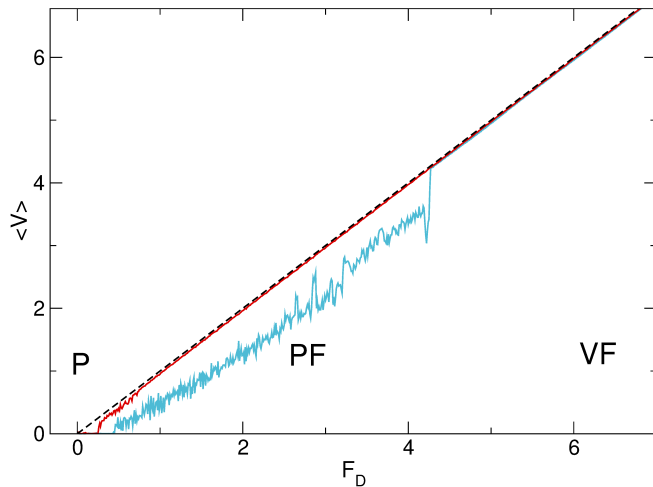


FIG. 10.  $\langle V \rangle$  vs  $F_D$  in the bubble state at  $B = 2.2$  for  $\rho = 0.52$  (blue) and  $\rho = 0.129$  (red). The pinned (P) state, plastic flow (PF) state, and viscous flow (VF) states are labeled for the  $\rho = 0.52$  system. The transition to viscous flow occurs at a much lower drive for the  $\rho = 0.129$  system where the bubbles are very small. The dashed line is the expected velocity-force curve for a free particle.

with a local maximum of the velocity and a dip in the depinning threshold. When the stripes are oriented, the probe particle is able to glide along the edge of a stripe, which we discuss in further detail below. The velocity is reduced in the void lattice state since the probe particle must break the particle-particle interaction bonds in order to move through the structure. In the crystal state,  $F_c$  grows with increasing  $\rho$  since the barrier to motion for high particle densities arises from the shorter range portion of the repulsive term in the interaction potential, and this barrier increases as the particles are pushed closer together. There is a jump up in velocity at the transition to the crystal state because the probe particle is able to establish a one-dimensional channel flow between the rows of the background lattice. For  $\rho > 1.6$ , the depinning transition becomes plastic and the velocity at the depinning transition drops due to the increased amount of plastic deformation; however, for drives greater than  $F_D = 1.0$ , there is a jump up in the velocity when the probe particle is able to transition to interstitial flow that does not induce plastic deformation in the surrounding medium. For systems with purely repulsive interactions, the depinning threshold increases monotonically and the velocity at fixed drive decreases monotonically with increasing  $\rho$ . For our competing interaction system, both the depinning threshold and the velocity at fixed drive change strongly nonmonotonically with increasing  $\rho$ .

We find distinctive flow regimes in the bubble system. In Fig. 10, we plot  $\langle V \rangle$  versus  $F_D$  for the bubble state at  $B = 2.2$  for densities of  $\rho = 0.52$  and  $\rho = 0.129$ , along with a dashed line indicating the expected response for a free particle. When  $\rho = 0.52$ , there is a pinned regime followed by a plastic flow (PF) regime with large velocity

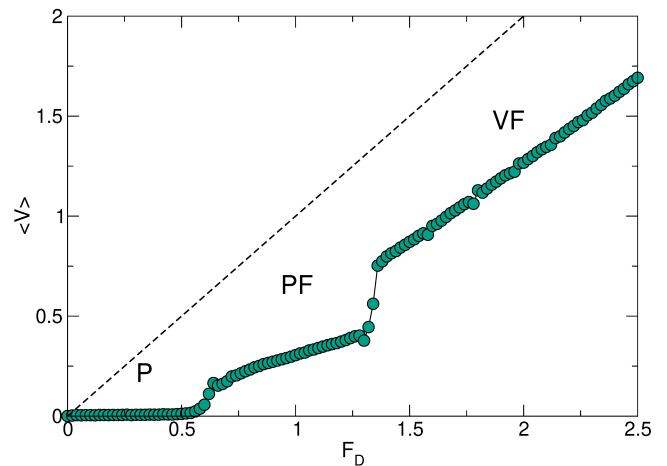


FIG. 11.  $\langle V \rangle$  vs  $F_D$  for a uniform crystal state at  $\rho = 1.38$  and  $B = 2.2$  showing a pinned (P) phase, a plastic flow (PF) phase, and a viscous flow (VF) phase. The dashed line is the expected velocity response for a free particle.

fluctuations and significant distortions in the surrounding media. At higher drives, the velocity jumps up nearly to the free flow value and the velocity fluctuations are strongly reduced. In this state, the probe particle is moving fast enough that the background particles cannot respond rapidly enough for plastic distortions to occur. We call this the viscous flow (VF) regime because the probe particle is still moving more slowly than a free particle since the interactions with the background particles enhance the effective viscosity. The onset of the viscous flow regime depends strongly on the type of pattern that forms. Generally, the PF-VF transition falls at low drive values for small  $\rho$ , and reaches its maximum value in the stripe regime. In Fig. 10, the PF-VF transition for  $\rho = 0.129$ , where the bubbles are small, occurs at a much lower value of  $F_D$  than for the  $\rho = 0.52$  system. When the bubbles are small, the amount of possible plastic deformation that can be produced by the moving probe particle is reduced, so a lower threshold drive is needed to eliminate the plastic deformations and produce the viscous flow state.

In the uniform crystal phase, there can also be a plastic flow (PF) regime just above depinning, as shown in Fig. 11 where we plot  $\langle V \rangle$  versus  $F_D$  for a crystal state at  $B = 2.2$  and  $\rho = 1.38$ . At higher drives, a transition to a VF regime occurs when the probe particle begins to move between the rows of the background particles. The velocity response is reduced in the PF regime due to the plastic distortions, and there is a jump up in the velocity at the transition to the VF regime. As  $\rho$  increases, the velocity in the VF regime decreases because the probe particle interacts with a greater number of background particles, resulting in a higher effective viscosity. Additionally, the velocity fluctuations in the PF regime are smaller for the uniform crystal state than in the bubble or stripe states since the plastic motion occurs in a more

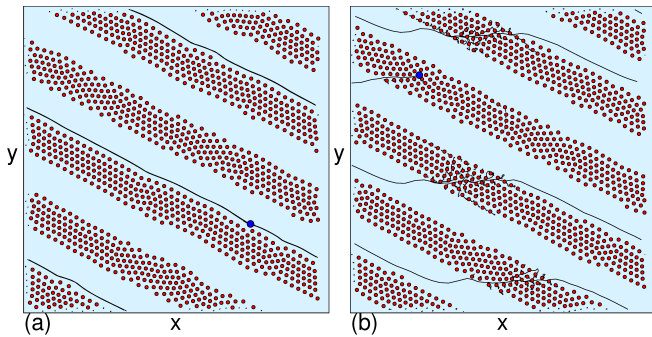


FIG. 12. Locations (dots) and trajectories (lines) of the probe particle (blue) and surrounding particles (red) in the stripe state at  $B = 2.2$  and  $\rho = 0.94$ . (a) At  $F_D = 0.5$ , the probe particle moves along the front edge of the stripe and does not follow the driving direction. (b)  $F_D = 1.05$ , just above the drive where the probe particle is able to break through the stripe and create plastic deformations.

correlated fashion in the uniform crystal.

Figure 9 shows that as  $\rho$  increases, two regimes of stripe states appear: disordered stripes for  $0.525 < \rho < 0.75$ , and oriented stripes for  $0.75 \leq \rho < 1.0$ . The initial depinning in the ordered stripe state occurs when the probe particle is able to escape from inside the stripe but cannot reenter the stripe, so that the particle runs along the edge of the stripe as illustrated in Fig. 12(a) for a system with  $B = 2.2$  and  $\rho = 0.94$  at  $F_D = 0.5$ . In this case, the probe particle is moving along the front edge of the stripe since the attractive portion of the potentials of the particles inside the stripe has captured the probe particle. This edge motion occurs without plastic deformations, and produces the large velocity in the stripe phase at fixed  $F_D = 1.0$  that is shown in Fig. 9(b). Since there is no mechanism that would cause the stripes to order along the  $x$  direction, when the probe particle follows the edge of the stripe it does not move along the driving direction but instead travels at an angle to the driving direction, resulting in the emergence of a finite Hall angle.

In Fig. 13(a), we plot  $\langle V \rangle$  and  $\langle V_y \rangle$  versus  $F_D$  for the stripe system from Fig. 12. The pinned regime is followed by what we term the Hall regime, where both the  $x$  and  $y$  velocities increase in magnitude with increasing  $F_D$ . A blowup of the Hall regime appears in Fig. 13(b). At high enough drives, the probe particle begins to break through the stripe and generate plastic rearrangements, causing a drop in magnitude of both the  $x$  and  $y$  velocity components due to the enhanced dissipation, as illustrated in Fig. 12(b) for  $F_D = 1.05$ . For drives just above this breakthrough transition, the probe particle still has a nonzero net  $y$  velocity, but  $\langle V_y \rangle$  gradually approaches zero at higher drives when the probe particle is moving fast enough to enter the viscous flow regime. The guided Hall regime motion is absent in the void lattice phase because the void lattice does not break symmetry across

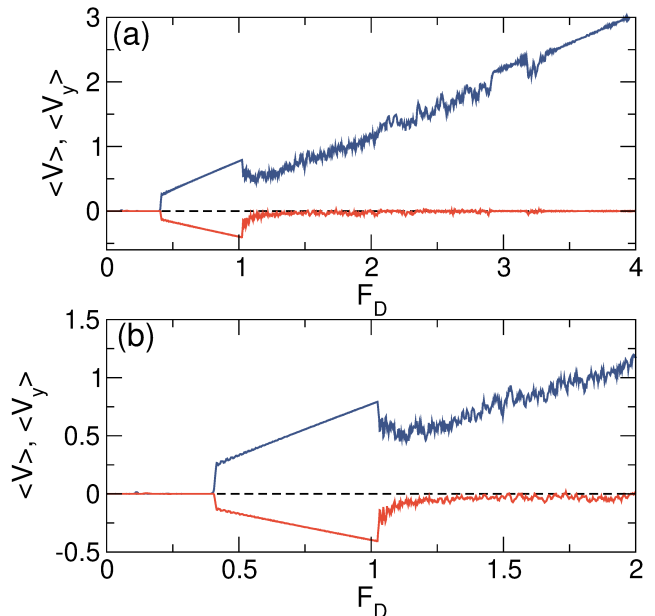


FIG. 13. (a)  $\langle V \rangle$  (blue) and  $\langle V_y \rangle$  (red) vs  $F_D$  for the system in Fig. 12 in the stripe state at  $B = 2.2$  and  $\rho = 0.94$ , showing a pinned phase, a Hall regime, a plastic flow regime, and a high drive viscous flow regime. (b) A blowup of the Hall regime from panel (a).

the  $y$ -direction. The particular orientation of the ordered stripe state depends on the initial conditions and how the system is prepared. Our results show that, in general, oriented stripes will produce a finite Hall angle since the drive on the probe particle is not likely to be perfectly aligned with the stripe orientation direction. The transition to the viscous flow state at high drives appears in Fig. 13(a) as a sudden change to a state with greatly reduced fluctuations in  $\langle V \rangle$ . There is a window of viscous flow beginning at  $F_D = 2.9$  that is interrupted by a temporary return to plastic flow at  $F_D = 3.17$ . The system then fully enters the viscous flow state at  $F_D = 3.35$ .

The Hall flow regime remains robust for other densities and  $B$  values. For example, in Fig. 14(a) we plot  $\langle V \rangle$  and  $\langle V_y \rangle$  for a high density oriented stripe system with  $B = 2.3$  and  $\rho = 1.66$ . The stripes are quite wide at this density, as shown in Fig. 15. The probe particle remains trapped in the stripe up to  $F_D = 0.9$ , indicating that it is difficult for the probe particle to escape from the wider stripe. The pinned state consists of two phases. In the first, which we call an elastic flow (EF) regime, the entire system is dragged in the direction of probe motion, as shown in Fig. 14(b) where we highlight  $\langle V \rangle$  and  $\langle V_y \rangle$  versus  $F_D$  at drives below the Hall regime. Only the  $x$  velocity of the probe particle is nonzero for  $F_D < 0.4$ . The jumps in  $\langle V \rangle$  and  $\langle V_y \rangle$  that appear in Fig. 14(b) are the result of brief large plastic rearrangements in which the probe particle shifts its position inside the stripe but remains trapped inside the stripe. For  $F_D \geq 0.4$ , the stripe that contains the probe

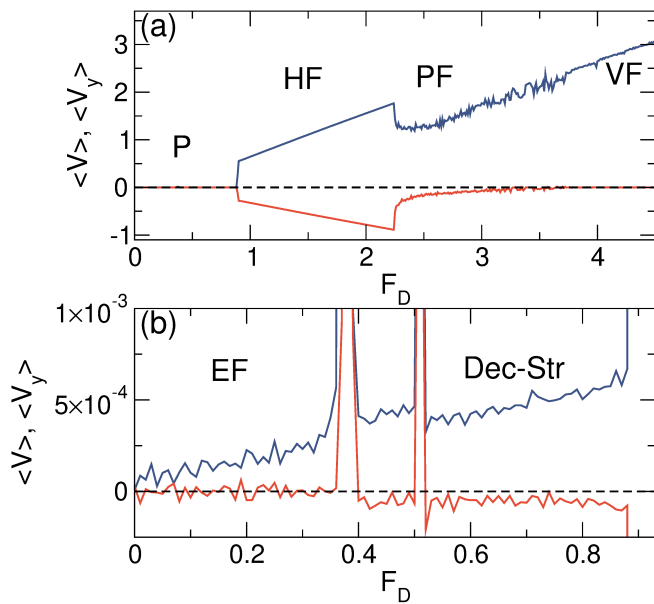


FIG. 14.  $\langle V \rangle$  (blue) and  $\langle V_y \rangle$  (red) vs  $F_D$  for the oriented stripe state at  $B = 2.3$  and  $\rho = 1.66$ . (a) The labeled regions are a pinned (P) phase where the probe particle remains trapped in the stripe, as illustrated in Fig. 15(a), the Hall flow (HF) regime shown in Fig. 15(b), a plastic flow (PF) phase imaged in Fig. 15(c), and a viscous flow (VF) regime shown in Fig. 15(d). (b) A blowup of the pinned phase from panel (a), consisting of an elastic flow (EF) state where all of the particles move very slowly together, and a decoupled stripe (Dec-Str) state in which the stripe containing the probe particle moves past the other stripes, as illustrated in Fig. 15(a).

particle breaks away from the other stripes and continues to move while the other stripes remain stationary, creating a decoupled stripe (Dec-Str) regime. The stripe containing the probe particle moves in the positive  $x$  and negative  $y$  direction, which is visible as the development of a finite  $\langle V_y \rangle$  that grows in magnitude in Fig. 14(b) over the range  $0.4 < F_D < 0.9$ . The Hall angle also becomes finite at this time. In Fig. 15(a), we illustrate the decoupled stripe phase at  $F_D = 0.7$  where the trajectories show that the motion occurs only in the stripe that contains the probe particle. In general, decoupled stripe states occur for large  $B$  and large stripe widths, where there is a more extensive range of  $F_D$  over which the probe particle can remain trapped inside the stripe. For  $0.9 < F_D < 2.25$ , the probe particle jumps out of the stripe and moves along the stripe edge, as shown in Fig. 15(b) at  $F_D = 1.5$ . In this Hall flow regime, the probe particle moves in the positive  $x$  and negative  $y$  direction but also drags the entire stripe in the positive  $y$  and positive  $x$  direction. For  $F_D > 2.25$ , the probe particle escapes from the stripe edge and becomes able to pass through the stripe, and the system enters the plastic flow regime, illustrated at  $F_D = 2.3$  in Fig. 15(c). When the probe particle breaks through the stripes, it creates plastic rearrangements within the stripe that reduce the

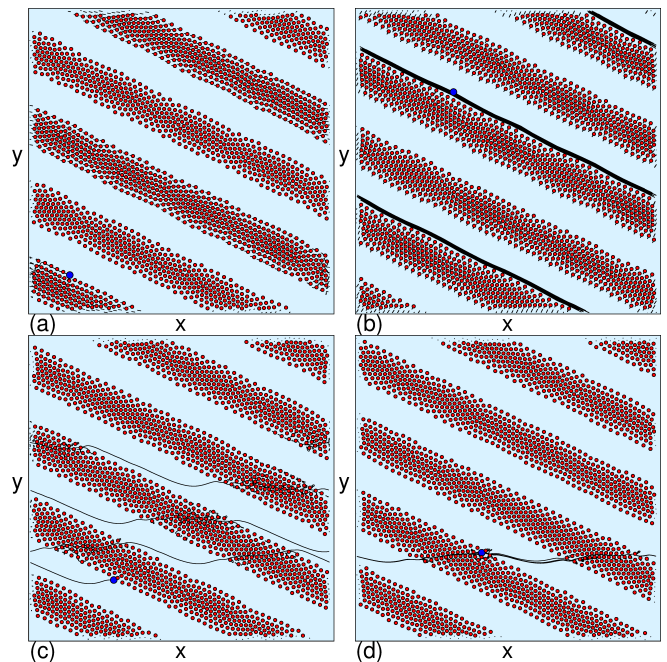


FIG. 15. Locations (dots) and trajectories (lines) of the probe particle (blue) and surrounding particles (red) in the ordered stripe state from Fig. 14 with  $B = 2.3$  and  $\rho = 1.66$ . (a) At  $F_D = 0.7$ , the probe particle is trapped inside a stripe and drags that stripe at an angle while the other stripes do not move in the stripe decoupled phase. (b)  $F_D = 1.5$  in the Hall flow regime, where the probe particle moves in the positive  $x$  and negative  $y$  direction, and the stripes are dragged in the positive  $y$  and positive  $x$  direction. (c)  $F_D = 2.3$  in the plastic flow regime. (d)  $F_D = 4.2$  in the viscous flow regime, where the probe particle does not create plastic deformations as it passes through the stripes.

velocity of the probe particle. The system remains in the plastic flow phase over the range  $2.25 < F_D < 3.72$ , and when  $F_D \geq 3.72$ , a viscous flow regime appears in which the probe particle moves so rapidly through the stripe that no large scale plastic rearrangements occur, as shown in Fig. 15(d) at  $F_D = 4.2$ .

From the velocity-force curves and the different dynamical phases, we can construct a dynamic phase diagram highlighting the pinned state, plastic flow, viscous flow, and Hall flow states, as shown in Fig. 16 as a function of  $F_D$  versus  $\rho$  for a system with  $B = 2.2$ . The vertical dashed lines indicate the separations between the bubble, stripe, void lattice, and uniform crystal states. The depinning threshold is non-monotonic as a function of  $B$ , as previously shown in Fig. 9. At low  $\rho$ , the transition from plastic flow to viscous flow occurs at a very low drive, while a local peak in the PF-VF transition appears slightly below the bubble to stripe boundary. As  $\rho$  is increased, the bubbles grow in size and can more effectively trap the probe particles, so a larger drive must be applied in order to reach the viscous flow regime. In the stripe phase, the PF-VF transition drops to lower values



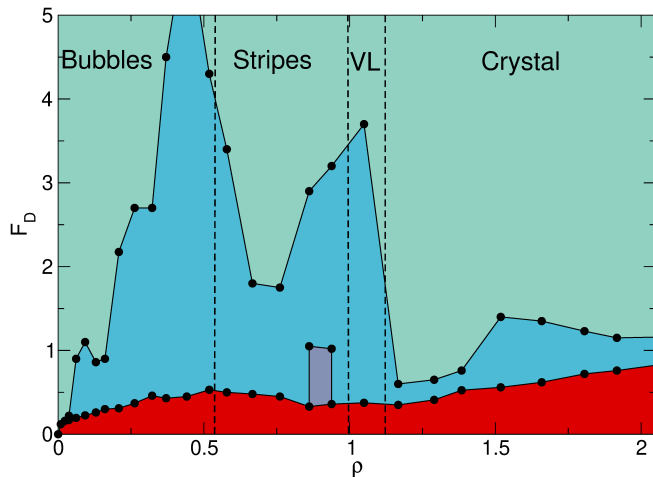


FIG. 16. Dynamic phase diagram as a function of  $F_D$  vs  $\rho$  at a fixed  $B = 2.2$  highlighting the pinned state (red), plastic flow (blue), viscous flow (green), and Hall flow (purple). The vertical lines indicate the separations between the bubble, stripe, void lattice (VL), and uniform crystal states.

because the probe particle is traveling through stripes that have a reduced width compared to the size of the bubbles at the upper edge of the bubble state. As  $\rho$  increases, the width of the stripes increases, and the extent of the plastic flow phase increases until the PF-VF transition reaches another local maximum just above the transition to the void lattice state. In the uniform crystal phase, the amount of plastic flow is greatly reduced and the PF-VF transition drops to a low value of  $F_D$ . The probe particle transitions to the viscous flow regime when it begins to move between the rows of particles in the background crystal. The guided Hall flow regime appears in a window where wide stripes are present, and occurs when the stripes form an aligned state instead of a disordered labyrinth state.

We next consider parameters for which the system exhibits only one dominant phase. In Fig. 17(a), we plot  $F_c$  versus  $\rho$  for a system with  $B = 1.6$ , which is in the uniform crystal phase for  $\rho > 0.15$ . Throughout the uniform crystal state,  $F_c$  increases monotonically with increasing  $\rho$ . Figure 17(b) shows the corresponding  $\langle V \rangle$  versus  $\rho$  curves for fixed drives of  $F_D = 1.0$  and  $2.0$ . Each curve is flat in the low density bubble and stripe phases, and gradually decreases with increasing  $\rho$  in the uniform crystal phase. At  $F_D = 1.0$ , when  $\rho > 1.4$  the probe particle is able to generate plastic deformations in the surrounding particles, producing a drop in  $\langle V \rangle$ . In contrast, at  $F_D = 2.0$  the drive is high enough that the probe particle always remains in the elastic flow regime, so there is no velocity drop at this drive. In Fig. 17(c) we plot  $F_c$  versus  $\rho$  for the same system at  $B = 2.4$ , where a bubble phase is present over the entire range of  $\rho$  values shown. Although  $F_c$  increases nearly monotonically with increasing  $\rho$ , there is a plateau near  $\rho = 1.0$  corresponding to the point at which the bubbles begin to merge into

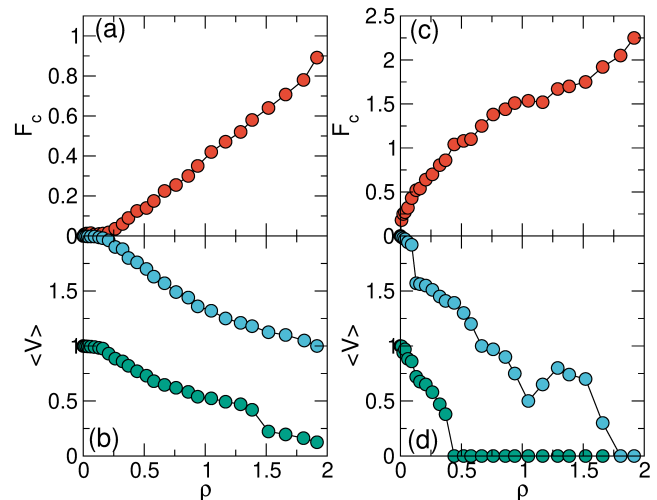


FIG. 17. (a)  $F_c$  vs  $\rho$  for a system with  $B = 1.6$ . The system is in the uniform crystal state for  $\rho > 0.15$ , and  $F_c$  increases monotonically with increasing  $\rho$  in this regime. (b) The corresponding  $\langle V \rangle$  vs  $\rho$  at fixed  $F_D = 1.0$  (green) and  $2.0$  (blue) shows a monotonic decrease with  $\rho$ . (c)  $F_c$  vs  $\rho$  for a system with  $B = 2.4$ , where the system is in a bubble phase for all values of  $\rho$ . (d) The corresponding  $\langle V \rangle$  vs  $\rho$  for fixed  $F_D = 1.0$  (green) and  $2.0$  (blue). When  $F_D = 2.0$ , the velocity has a non-monotonic dependence on  $\rho$ .

elongated objects. Figure 17(d) shows the corresponding  $\langle V \rangle$  at  $F_D = 1.0$  and  $F_D = 2.0$ . At both drives, when  $\rho < 0.1$ , the probe particle rapidly moves from bubble to bubble in a viscous flow regime, so there are no plastic distortions. When  $F_D = 1.0$ , the probe particle remains trapped inside a bubble for  $\rho > 0.4$ , while at  $F_D = 2.0$ , the probe particle is trapped for  $\rho > 1.75$ .

#### IV. DISCUSSION

In this work, the competing interaction potential we considered involved Coulomb repulsion combined with exponential attraction; however, many other types of competing interactions are possible, such as a Yukawa repulsion and/or a power law attraction. The formation of crystal, stripe, and bubble states remains robust for a wide range of interaction potentials, including purely repulsive potentials that have two distinct length scales [30]. Therefore, we expect many of the same active rheology effects observed here to be relevant for particles with other types of competing interactions, and an exploration of alternative interactions would be an interesting direction for future work. We considered a dc driven probe particle, but it would also be interesting to study ac driven particles to look for resonant frequency effects, or to combine dc and ac driving to see whether ac shaking increases or decreases the effective drag on the probe particle. We studied the situation of constant driving force, but it is also possible to consider a probe particle that

moves with constant velocity. In that case, the presence of different states would produce different force fluctuations of the probe particle. Viscous flow states would give only small force fluctuations, while plastic flows would be associated with strong force fluctuations. We also did not consider thermal effects. These could be interesting since many of the phases we observe might exhibit one creep rate during inter-bubble or inter-stripe motion, but have a different creep rate for hopping from stripe to stripe or bubble to bubble. This system is also likely to have multiple-step melting transitions, so a probe particle subjected to constant driving would show upward or downward jumps in the viscosity as the temperature is varied [3].

## V. SUMMARY

We have investigated active rheology for a probe particle moving through a pattern forming system of particles with competing long-range repulsion and short-range attraction. The probe particle is driven at constant force, and we measure the threshold force needed for motion as well as the velocity response as the attractive term or the particle density is varied. For a fixed density, the system forms uniform crystal, stripe, and bubble lattice states as a function of increasing attraction. The threshold force is a nonmonotonic function of the attractive term and passes through a minimum at the transition from uniform crystal to stripe. The threshold then increases with increasing attraction in the bubble phase. In the uniform crystal state, the probe particle can travel between the rows of particles, while in the stripe and bubble states, the probe particle can be pinned within a stripe or bubble, and upon depinning is able to jump from stripe to stripe or bubble to bubble. For a fixed drive above the depinning threshold, as the attraction is increased, the velocity has a local maximum at the transition from bubbles to stripes where the attractive and repulsive forces are the most balanced and the trapping effect on the probe particle reaches its lowest value. We

observe multiple dynamical regimes above depinning that involve different amounts of plastic deformations induced in the surrounding particles by the moving probe particle. For sufficiently large driving forces, the probe particle moves so rapidly through the background that the surrounding particles do not have enough time to respond via plastic deformations, and the probe particle enters a viscous flow state where plastic deformation is absent and the effective drag is reduced. When the attractive term is held fixed and the particle density is increased, we observe transitions among bubble, stripe, void lattice, and uniform crystal states. The threshold for probe particle motion changes nonmonotonically with particle density as the system passes through the different patterned states. For fixed driving above threshold, the effective drag is nonmonotonic, and shows jumps and dips across the different structural transitions. For some parameter values, we find disordered or labyrinthine stripe patterns, while for other parameter values, the stripes collectively orient into an ordered state. A probe particle moving through oriented stripes can flow easily along the edge of the stripe, resulting in a regime of finite Hall angle motion. At higher drives, the probe particle breaks through the stripe, leading to a drop in the velocity or an enhancement of the drag. We map out a dynamical phase diagram as a function of drive and density for fixed attraction. Our results should be relevant to a variety of systems with competing long-range repulsion and short-range attraction in both soft and hard condensed matter.

## ACKNOWLEDGMENTS

We gratefully acknowledge the support of the U.S. Department of Energy through the LANL/LDRD program for this work. This work was supported by the US Department of Energy through the Los Alamos National Laboratory. Los Alamos National Laboratory is operated by Triad National Security, LLC, for the National Nuclear Security Administration of the U. S. Department of Energy (Contract No. 892333218NCA000001).

- 
- [1] M. B. Hastings, C. J. Olson Reichhardt, and C. Reichhardt, Depinning by fracture in a glassy background, *Phys. Rev. Lett.* **90**, 098302 (2003).
  - [2] P. Habdas, D. Schaar, A. C. Levitt, and E. R. Weeks, Forced motion of a probe particle near the colloidal glass transition, *Europhys. Lett.* **67**, 477 (2004).
  - [3] C. Reichhardt and C. J. O. Reichhardt, Local melting and drag for a particle driven through a colloidal crystal, *Phys. Rev. Lett.* **92**, 108301 (2004).
  - [4] T. M. Squires and J. F. Brady, A simple paradigm for active and nonlinear microrheology, *Phys. Fluids* **17**, 073101 (2005).
  - [5] I. Gazuz, A. M. Puertas, T. Voigtmann, and M. Fuchs, Active and nonlinear microrheology in dense colloidal suspensions, *Phys. Rev. Lett.* **102**, 248302 (2009).
  - [6] A. S. Khair and T. M. Squires, Active microrheology: A proposed technique to measure normal stress coefficients of complex fluids, *Phys. Rev. Lett.* **105**, 156001 (2010).
  - [7] D. Winter, J. Horbach, P. Virnau, and K. Binder, Active nonlinear microrheology in a glass-forming Yukawa fluid, *Phys. Rev. Lett.* **108**, 028303 (2012).
  - [8] D. Anderson, D. Schaar, H. G. E. Hentschel, J. Hay, P. Habdas, and E. R. Weeks, Local elastic response measured near the colloidal glass transition, *J. Chem. Phys.* **138**, 12A520 (2013).
  - [9] J. W. Swan and R. N. Zia, Active microrheology: fixed-velocity versus fixed-force, *Phys. Fluids* **25**, 083303 (2013).
  - [10] O. Benichou, P. Illien, C. Mejia-Monasterio, and G. Oshanin, A biased intruder in a dense quiescent medium:

- looking beyond the force-velocity relation, *J. Stat. Mech.* **2013**, P05008 (2013).
- [11] A. M. Puertas and T. Voigtmann, Microrheology of colloidal systems, *J. Phys.: Condens. Matter* **26**, 243101 (2014).
- [12] M. Gruber, G. C. Abade, A. M. Puertas, and M. Fuchs, Active microrheology in a colloidal glass, *Phys. Rev. E* **94**, 042602 (2016).
- [13] R. Wulfert, U. Seifert, and T. Speck, Nonequilibrium depletion interactions in active microrheology, *Soft Matter* **13**, 9093 (2017).
- [14] R. N. Zia, Active and passive microrheology: Theory and simulation, *Ann. Rev. Fluid Mech.* **50**, 371 (2018).
- [15] J. W. Yu, S. H. E. Rahbari, T. Kawasaki, H. Park, and W. B. Lee, Active microrheology of a bulk metallic glass, *Sci. Adv.* **6**, 10.1126/sciadv.aba8766 (2020).
- [16] N. Şenbil, M. Gruber, C. Zhang, M. Fuchs, and F. Schefold, Observation of strongly heterogeneous dynamics at the depinning transition in a colloidal glass, *Phys. Rev. Lett.* **122**, 108002 (2019).
- [17] M. Gruber, A. M. Puertas, and M. Fuchs, Critical force in active microrheology, *Phys. Rev. E* **101**, 012612 (2020).
- [18] A. Hopkins, M. Chiang, B. Loewe, D. Marenduzzo, and M. C. Marchetti, Local yield and compliance in active cell monolayers, *Phys. Rev. Lett.* **129**, 148101 (2022).
- [19] J. A. Drocco, M. B. Hastings, C. J. O. Reichhardt, and C. Reichhardt, Multiscaling at point  $J$ : Jamming is a critical phenomenon, *Phys. Rev. Lett.* **95**, 088001 (2005).
- [20] R. Candelier and O. Dauchot, Journey of an intruder through the fluidization and jamming transitions of a dense granular media, *Phys. Rev. E* **81**, 011304 (2010).
- [21] E. Kolb, P. Cixous, N. Gaudouen, and T. Darnige, Rigid intruder inside a two-dimensional dense granular flow: Drag force and cavity formation, *Phys. Rev. E* **87**, 032207 (2013).
- [22] C. Reichhardt and C. J. O. Reichhardt, Active microrheology, Hall effect, and jamming in chiral fluids, *Phys. Rev. E* **100**, 012604 (2019).
- [23] C. Duclut, S. Bo, R. Lier, J. Armas, P. Surówka, and F. Jülicher, Probe particles in odd active viscoelastic fluids: How activity and dissipation determine linear stability, *Phys. Rev. E* **109**, 044126 (2024).
- [24] C. Reichhardt and C. J. O. Reichhardt, Active microrheology in active matter systems: Mobility, intermittency, and avalanches, *Phys. Rev. E* **91**, 032313 (2015).
- [25] E. W. J. Straver, J. E. Hoffman, O. M. Auslaender, D. Rugar, and K. A. Moler, Controlled manipulation of individual vortices in a superconductor, *Appl. Phys. Lett.* **93**, 172514 (2008).
- [26] O. M. Auslaender, L. Luan, E. W. J. Straver, J. E. Hoffman, N. C. Koshnick, E. Zeldov, D. A. Bonn, R. Liang, W. N. Hardy, and K. A. Moler, Mechanics of individual isolated vortices in a cuprate superconductor, *Nature Phys.* **5**, 35 (2009).
- [27] C. Reichhardt, Vortices wiggled and dragged, *Nature Phys.* **5**, 15 (2009).
- [28] X.-G. Wang, L. Chotorlishvili, V. K. Dugaev, A. Ernst, I. V. Maznichenko, N. Arnold, C. Jia, J. Berakdar, I. Mertig, and J. Barnaš, The optical tweezer of skyrmions, *npj Comput. Mater.* **6**, 140 (2020).
- [29] C. Reichhardt and C. J. O. Reichhardt, Dynamics and nonmonotonic drag for individually driven skyrmions, *Phys. Rev. B* **104**, 064441 (2021).
- [30] M. Seul and D. Andelman, Domain shapes and patterns - the phenomenology of modulated phases, *Science* **267**, 476 (1995).
- [31] A. D. Stoycheva and S. J. Singer, Stripe melting in a two-dimensional system with competing interactions, *Phys. Rev. Lett.* **84**, 4657 (2000).
- [32] C. Reichhardt, C. J. Olson, I. Martin, and A. R. Bishop, Depinning and dynamics of systems with competing interactions in quenched disorder, *Europhys. Lett.* **61**, 221 (2003).
- [33] C. J. O. Reichhardt, C. Reichhardt, I. Martin, and A. R. Bishop, Dynamics and melting of stripes, crystals, and bubbles with quenched disorder, *Physica D* **193**, 303 (2004).
- [34] S. Mossa, F. Sciortino, P. Tartaglia, and E. Zaccarelli, Ground-state clusters for short-range attractive and long-range repulsive potentials, *Langmuir* **20**, 10756 (2004).
- [35] F. Sciortino, S. Mossa, E. Zaccarelli, and P. Tartaglia, Equilibrium cluster phases and low-density arrested disordered states: The role of short-range attraction and long-range repulsion, *Phys. Rev. Lett.* **93**, 055701 (2004).
- [36] K. Nelissen, B. Partoens, and F. M. Peeters, Bubble, stripe, and ring phases in a two-dimensional cluster with competing interactions, *Phys. Rev. E* **71**, 066204 (2005).
- [37] Y. H. Liu, L. Y. Chew, and M. Y. Yu, Self-assembly of complex structures in a two-dimensional system with competing interaction forces, *Phys. Rev. E* **78**, 066405 (2008).
- [38] C. J. Olson Reichhardt, C. Reichhardt, and A. R. Bishop, Structural transitions, melting, and intermediate phases for stripe- and clump-forming systems, *Phys. Rev. E* **82**, 041502 (2010).
- [39] D. McDermott, C. J. O. Reichhardt, and C. Reichhardt, Stripe systems with competing interactions on quasi-one dimensional periodic substrates, *Soft Matter* **10**, 6332 (2014).
- [40] Y. Liu and Y. Xi, Colloidal systems with a short-range attraction and long-range repulsion: phase diagrams, structures, and dynamics, *Curr. Opin. Colloid Interf. Sci.* **19**, 123 (2019).
- [41] A. Al Harraq, A. A. Hymel, E. Lin, T. M. Truskett, and B. Bharti, Dual nature of magnetic nanoparticle dispersions enables control over short-range attraction and long-range repulsion interactions, *Commun. Chem.* **5**, 72 (2022).
- [42] A. Hooshanginejad, J.-W. Barotta, V. Spradlin, G. Pucci, R. Hunt, and D. M. Harris, Interactions and pattern formation in a macroscopic magnetocapillary salt system of mermaid cereal, *Nature Commun.* **15**, 5466 (2024).
- [43] E. A. Jagla, Phase behavior of a system of particles with core collapse, *Phys. Rev. E* **58**, 1478 (1998).
- [44] G. Malescio and G. Pellicane, Stripe phases from isotropic repulsive interactions, *Nature Mater.* **2**, 97 (2003).
- [45] M. A. Glaser, G. M. Grason, R. D. Kamien, A. Kosmrlj, C. D. Santangelo, and P. Ziherl, Soft spheres make more mesophases, *EPL* **78**, 46004 (2007).
- [46] L. Q. Costa Campos, S. W. S. Apolinario, and H. Löwen, Structural ordering of trapped colloids with competing interactions, *Phys. Rev. E* **88**, 042313 (2013).
- [47] M. M. Fogler, A. A. Koulakov, and B. I. Shklovskii, Ground state of a two-dimensional electron liquid in a weak magnetic field, *Phys. Rev. B* **54**, 1853 (1996).

- [48] R. Moessner and J. T. Chalker, Exact results for interacting electrons in high Landau levels, *Phys. Rev. B* **54**, 5006 (1996).
- [49] K. B. Cooper, M. P. Lilly, J. P. Eisenstein, L. N. Pfeiffer, and K. W. West, Insulating phases of two-dimensional electrons in high Landau levels: Observation of sharp thresholds to conduction, *Phys. Rev. B* **60**, R11285 (1999).
- [50] E. Fradkin and S. A. Kivelson, Liquid-crystal phases of quantum Hall systems, *Phys. Rev. B* **59**, 8065 (1999).
- [51] J. Göres, G. Gamez, J. H. Smet, L. Pfeiffer, K. West, A. Yacoby, V. Umansky, and K. von Klitzing, Current-induced anisotropy and reordering of the electron liquid-crystal phases in a two-dimensional electron system, *Phys. Rev. Lett.* **99**, 246402 (2007).
- [52] H. Zhu, G. Sambandamurthy, L. W. Engel, D. C. Tsui, L. N. Pfeiffer, and K. W. West, Pinning mode resonances of 2D electron stripe phases: Effect of an in-plane magnetic field, *Phys. Rev. Lett.* **102**, 136804 (2009).
- [53] B. Friess, V. Umansky, K. von Klitzing, and J. H. Smet, Current flow in the bubble and stripe phases, *Phys. Rev. Lett.* **120**, 137603 (2018).
- [54] J. M. Tranquada, B. J. Sterlieb, J. D. Axe, Y. Nakamura, and S. Uchida, Evidence for stripe correlations of spins and holes in copper-oxide superconductors, *Nature (London)* **375**, 561 (1995).
- [55] C. J. Olson Reichhardt, C. Reichhardt, and A. R. Bishop, Fibrillar templates and soft phases in systems with short-range dipolar and long-range interactions, *Phys. Rev. Lett.* **92**, 016801 (2004).
- [56] T. Mertelj, V. V. Kabanov, and D. Mihailovic, Charged particles on a two-dimensional lattice subject to anisotropic Jahn-Teller interactions, *Phys. Rev. Lett.* **94**, 147003 (2005).
- [57] X. B. Xu, H. Fangohr, S. Y. Ding, F. Zhou, X. N. Xu, Z. H. Wang, M. Gu, D. Q. Shi, and S. X. Dou, Phase diagram of vortex matter of type-II superconductors, *Phys. Rev. B* **83**, 014501 (2011).
- [58] L. Komendová, M. V. Milošević, and F. M. Peeters, Soft vortex matter in a type-I/type-II superconducting bilayer, *Phys. Rev. B* **88**, 094515 (2013).
- [59] C. N. Varney, K. A. H. Sellin, Q.-Z. Wang, H. Fangohr, and E. Babaev, Hierarchical structure formation in layered superconducting systems with multi-scale inter-vortex interactions, *J. Phys.: Condens. Matter* **25**, 415702 (2013).
- [60] K. A. H. Sellin and E. Babaev, Stripe, gossamer, and glassy phases in systems with strong nonpairwise interactions, *Phys. Rev. E* **88**, 042305 (2013).
- [61] X. S. Brems, S. Mühlbauer, W. Y. Córdoba-Camacho, A. A. Shantenko, A. Vagov, J. A. Aguiar, and R. Cubitt, Current-induced self-organisation of mixed superconducting states, *Supercond. Sci. Technol.* **35**, 035003 (2022).
- [62] C. Reichhardt, C. J. O. Reichhardt, and M. Milosevic, Statics and dynamics of skyrmions interacting with disorder and nanostructures, *Rev. Mod. Phys.* **94**, 035005 (2022).
- [63] D. McDermott, C. J. O. Reichhardt, and C. Reichhardt, Structural transitions and hysteresis in clump- and stripe-forming systems under dynamic compression, *Soft Matter* **12**, 9549 (2016).
- [64] C. Reichhardt and C. J. O. Reichhardt, Peak effect and dynamics of stripe- and pattern-forming systems on a periodic one-dimensional substrate, *Phys. Rev. E* **109**, 054606 (2024).
- [65] C. Reichhardt, C. J. O. Reichhardt, I. Martin, and A. R. Bishop, Dynamical ordering of driven stripe phases in quenched disorder, *Phys. Rev. Lett.* **90**, 026401 (2003).